Transport in Porous Media (2022) 141:231–253
https://doi.org/10.1007/s11242-021-01722-y

Long-Term Redistribution of Residual Gas Due to Non-convective Transport in the Aqueous Phase

Yaxin Li[1] · **Franklin M. Orr Jr.**[1] · **Sally M. Benson**[1]

Received: 23 June 2021 / Accepted: 19 November 2021 / Published online: 26 November 2021

Abstract
Geological CO_2 sequestration is an effective approach to mitigate greenhouse gas emissions by permanently trapping CO_2 in the subsurface. A large portion of injected CO_2 is trapped by capillary forces in pores and eventually dissolves into the reservoir brine due to convective mixing to achieve permanent entrapment. In regions where convective mixing is slow, non-convective transport can play an important role in redistributing residually trapped CO_2, but the mechanisms and timescales for redistribution have yet to be explored thoroughly. In previous work, we have shown that capillary pressure difference among residually trapped gas ganglia can induce Ostwald ripening, thereby redistributing the separate-phase gas through diffusion despite the gas phase remaining trapped over the entire course of equilibration. In this study, we show from a thermodynamic point of view that other natural gradients in geologic formations— hydrostatic pressure, geothermal gradients and capillary heterogeneity—can also redistribute CO_2 by non-convective transport. Mechanisms for resulting non-convective transport include molecular diffusion, the sedimentation effect and potentially the Soret effect. Results show that hydrostatic pressure dominates redistribution such that the separate-phase gas is transported upward through molecular diffusion and accumulates under the seal at the steady state. A typical timescale for gas phase redistribution is 10^5 years/m; for a 100-m-thick formation, redistribution is complete after $\sim 10^7$ years. Although non-convective transport is an extremely slow process, it causes local accumulation of the gas phase and in some settings may remobilize the trapped gas phase.

Keywords Residual trapping · Thermodynamic equilibrium · Non-convective transport · CO_2 sequestration

1 Introduction

In a geological formation where a continuous gas phase migrates due to buoyancy forces, formation brine imbibes into the trailing edge of the gas plume. During imbibition, the gas phase at the trailing edge becomes disconnected into many individual gas ganglia that

✉ Yaxin Li
yaxinl@stanford.edu

[1] Department of Energy Resources Engineering, Stanford University, Stanford, CA, USA

are trapped in the pore spaces. This trapping mechanism is referred to as residual trapping (Roof 1970; Kumar et al. 2004; Mo et al. 2005; Hesse et al. 2006; Juanes et al. 2006; Suekane et al. 2008; Iglauer et al. 2011; Krevor et al. 2012). Residually trapped gas widely exists along the migration path of the gas phase in many natural geological formations, such as oil and gas reservoirs, methane-rich undersea sediments and saline formations for geological storage of CO_2 (Claypool and Kaplan 1974; Chatzis et al. 1983; Kumar et al. 2005; Lei and Seol 2020).

In the context of geological CO_2 storage, the long-term entrapment of residually trapped gas enhances the security of CO_2 storage, since residually trapped CO_2 can immobilize a large portion of injected CO_2Pentland et al. (2011); Burnside and Naylor (2014). One theory for the long-term fate of residually trapped CO_2 is that the separate-phase CO_2 will eventually dissolve into the formation brine, a process that is accelerated by convective mixing Bourg et al. (2015); Jiang and Tsuji (2015). Convective mixing originates from the fact that the aqueous solution of CO_2 near the top of the aquifer is slightly denser than the "fresh" brine underneathTeng et al. (1997). This density contrast drives the CO_2 solution to sink and brings more "fresh" brine into contact with separate-phase CO_2, thereby enhancing CO_2 dissolution Ennis-King et al. (2005); Riaz et al. (2006); Hassanzadeh et al. (2007); Neufeld et al. (2010). Studies have shown that the timescale for onset of convective mixing strongly depends on Rayleigh number, a combination of reservoir conditions and fluid properties Ennis-King et al. (2003). For reservoirs with low permeability ($k < 10$ mD), dissolution of residually trapped CO_2 is likely to be a slow process, occurring in thousands of years or longer after injection of CO_2Riaz et al. (2006).

Non-convective transport of dissolved gas in the aqueous phase and its impact on the separate-phase gas have drawn little attention. Examples of non-convective transport of dissolved gas include molecular diffusion due to concentration gradients, sedimentation of solute molecules in the gravitational field, the Soret effect due to heat flow in the system Mashimo (1988); Goldobin and Brilliantov (2011). As shown in Fig. 1, convective mixing mainly occurs in regions where the CO_2-saturated brine is in significant contact with the "fresh" brine; however, in regions containing a large amount of residually trapped gas, the aqueous phase is saturated with dissolved CO_2, and the contact with "fresh" brine is limited. In these regions, convective mixing will be extremely slow due to significantly lower density contrast in the aqueous phase. We have previously shown that non-convective transport due to Ostwald ripening in heterogeneous porous media can result in gas saturation changes on the timescale of years Li et al. (2020). Over the long term, the impacts of non-convective transport can accumulate and potentially play an important role in redistributing the residually trapped gas. Since geological CO_2 storage aims at permanent entrapment of CO_2, it is important to understand these non-convective processes and assess their significance for the security of CO_2 storage.

The first attempt to quantify non-convective transport in geological formations was performed in a system containing brine and residually trapped methane bubbles Goldobin and Brilliantov (2011). The authors show mathematically that in the presence of trapped methane bubbles, methane molecules dissolved in the aqueous phase are out of thermodynamic equilibrium, which create a driving force for non-convective transport of methane molecules in the aqueous phase. The authors neglect its influence on the separate-phase methane by simply treating the trapped methane bubbles as "infinite" sources. Recently, several studies have shown that non-convective transport of dissolved gas can change the distribution of residually trapped gas throughout the system, while the residual gas remains trapped and immobile over the entire course of equilibration. One mechanism for gas redistribution is Ostwald ripening due to capillary pressure difference among trapped gas. The

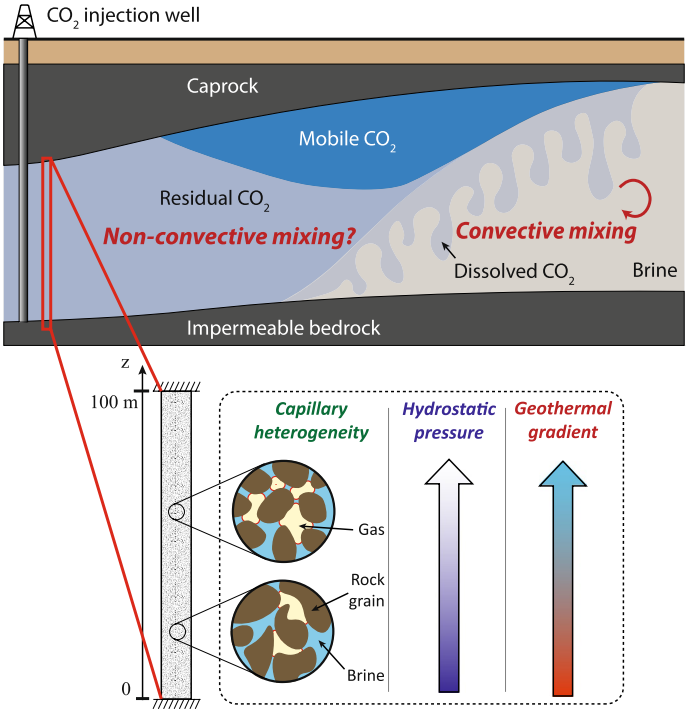

Fig. 1 A conceptual illustration of a CO_2 sequestration aquifer and the system this study focuses on. Convective mixing occurs in the regions where the mobile plume of CO_2 is in contact with a large amount of "fresh" brine to enhance CO_2 dissolution into the aquifer. In regions where little "fresh" brine is available to induce significant convective mixing, we study the non-convective transport of CO_2 dissolved in the aqueous phase and its impact on the long-term fate of residually trapped CO_2. Non-convective transport can result from hydrostatic pressure, geothermal gradients and capillary heterogeneity. By neglecting any regional flow of groundwater, the studies system is reduced to a one-dimensional closed column with residually trapped gas throughout the system initially

gradient of capillary pressure throughout the system induces inter-ganglion diffusion of gas molecules in the aqueous phase, causing trapped gas ganglia to grow or shrink. At steady state, all the gas ganglia in the system approach the equilibrium capillary pressure and coexist stably due to presence of the porous matrix (Garing et al. 2017; Xu et al. 2017; de Chalendar et al. 2018, 2019; Li et al. 2020). Another mechanism for non-convective transport is the sedimentation effect, where dissolved CO_2 molecules drift in the aqueous solution due to gravity, making trapped gas bubbles aligned in the direction of gravity re-equilibrate Xu et al. (2019).

These relevant studies have focused on only one specific type of non-convective transport at a time, when in reality a number of non-convective processes are occurring simultaneously. In fact, many natural gradients in geological formations can cause thermodynamic disequilibrium to potentially induce non-convective transport, including hydrostatic pressure (Muskat 1930; Sage and Lacey 1939), geothermal gradients (Schulte et al. 1980; Whitson et al. 1994; Padua 1999; Espósito et al. 2000; Galliero et al. 2016) and capillary heterogeneity at the continuum scale Pini et al. (2012). In addition, simplifications such as the ideal-solution assumption can yield results deviating significantly from that in real

fluids. Therefore, current studies do not quantify the significance of non-convective transport and its impact on residually trapped gas. These limitations necessitate a systematic approach for evaluating non-convective transport from a fundamental perspective.

Despite the limitations of these studies, their conclusions suggest that residually trapped gas may not remain trapped and disconnected over the long term, even without any convective flow. At the pore scale, the mass of residually trapped gas ganglia is redistributed through non-convective transport in the aqueous phase while the ganglia remain immobileGaring et al. (2017), Xu et al. (2017), de Chalendar et al. (2018, 2019), at the continuum scale, this redistribution results in saturation change of the gas phase throughout the system Xu et al. (2019), Li et al. (2020). In regions where the saturation of residual gas increases, these initially disconnected, residually trapped gas ganglia can aggregate and potentially become remobilized and migrate into different locations in the storage reservoir. Therefore, it is important to characterize non-convective transport in the presence of residually trapped gas. Understanding how these processes in turn affect the distribution of residually trapped gas and at what timescales in real geological systems are important problems to be addressed.

To fill this knowledge gap, we develop a fundamental description of non-convective transport of dissolved gas from a thermodynamic point of view, integrating the impact of hydrostatic pressure, geothermal gradient, the sedimentation effect and capillary heterogeneity. In this paper, residual gas redistribution through non-convective transport is demonstrated and characterized by numerical solutions within various systems. We report the timescale for resulting gas redistribution and its influence on long-term gas migration in geological formations. Lastly, we compare the relative significance of non-convective transport and convective mixing.

2 Non-convective Transport in the Aqueous Phase Due to the Gradients of Thermodynamic Potential

2.1 Basic Theory

As shown in Fig. 1, this study focuses on a two-phase fluid system in a porous medium, where the aqueous phase is continuous and the gas phase is residually trapped. The gas phase remains dispersed and immobile during the entire equilibration process. Therefore, the gas phase is redistributed only through non-convective transport in the aqueous phase. By neglecting any convective flow of the aqueous phase such as regional flow of groundwater, the system is reduced to a one-dimensional vertical column. We take water and supercritical CO_2 at reservoir conditions as an example fluid pair; however, this theory can be equally well applied to any non-reacting binary mixtures that are mutually soluble.

2.1.1 Equilibrium Condition Under Isothermal Condition

We focus on the thermodynamic potential of CO_2 dissolved in the aqueous phase, which consists mostly of free CO_2 molecules due to low pH in the aqueous phase Peng et al. (2013). We assume that the residual gas and aqueous phases are at equilibrium, so that the concentration of dissolved CO_2 is the CO_2 solubility at the local reservoir conditions. We define the partial molar free energy of dissolved CO_2 as $F^{aq}_{CO_2}$. In the aqueous phase, the criteria for equilibrium under isothermal condition in a centrifugal field (gravity in this

case) can be written as Muskat (1930); Sage and Lacey (1939); Schulte et al. (1980); Whitson et al. (1994); Firoozabadi (2016)

$$dT = 0, \tag{1}$$

$$dP = -\rho_w g dz, \tag{2}$$

$$dF^{aq}_{CO_2} = d\left(\mu^{aq}_{CO_2} + M_{CO_2} gz\right) = 0, \tag{3}$$

where T is temperature, P is pressure, ρ_w is the density of water, g is gravitational acceleration, z is elevation, $\mu^{aq}_{CO_2}$ is the chemical potential of CO_2 molecules dissolved in the aqueous phase, and M_{CO_2} is the molar weight of CO_2 molecules.

The chemical potential is dependent on both composition and pressure, i.e.,

$$d\mu^{aq}_{CO_2} = \left(\frac{\partial \mu^{aq}_{CO_2}}{\partial x_{CO_2}}\right)\Big|_P dx_{CO_2} + \left(\frac{\partial \mu^{aq}_{CO_2}}{\partial P}\right)\Big|_{x_{CO_2}} dP, \tag{4}$$

where x_{CO_2} is the mole fraction of CO_2 in the aqueous phase. The composition-dependent part of the chemical potential can be written as

$$\mu^{aq}_{CO_2}\left(x_{CO_2}\right)\Big|_P = \mu_0 + RTln\left(\gamma_{CO_2} x_{CO_2}\right), \tag{5}$$

where μ_0 is the chemical potential of pure CO_2 as a reference, R is the gas constant, and γ_{CO_2} is the activity coefficient of CO_2. Due to the low concentration of CO_2 in the aqueous phase (approximately 2% in mole fraction) at reservoir conditions, the activity coefficient can be approximated as a constant $\gamma = 55.508$, which is independent of concentration x_{CO_2} Spycher et al. (2003). As a result, $\frac{\partial \gamma_{CO_2}}{\partial x_{CO_2}}$ is approximated as 0 in our interested range of temperature and pressure. Therefore, the first term in RHS of Eq. 4 can be written as

$$\left(\frac{\partial \mu^{aq}_{CO_2}}{\partial x_{CO_2}}\right)\Big|_P dx_{CO_2} = \frac{RT}{x_{CO_2}} dx_{CO_2}. \tag{6}$$

In the second term in RHS of Eq. 4, $\frac{\partial \mu^{aq}_{CO_2}}{\partial P}\Big|_{x_{CO_2}}$ equals to $\bar{V}_{CO_2}$, the partial molar volume of dissolved CO_2 according to the second law of thermodynamics Sage and Lacey (1939); Goldberg (1953). Combining Eq. 2, the second term in RHS of Eq. 4 can be written as

$$\left(\frac{\partial \mu^{aq}_{CO_2}}{\partial P}\right)\Big|_{x_{CO_2}} dP = -\bar{V}_{CO_2} \rho_w g dz. \tag{7}$$

Substitute Eqs. 4, 6 and 7 into Eq. 3, we obtain the equilibrium condition, i.e.,

$$dF^{aq}_{CO_2} = \frac{RT}{x_{CO_2}} dx_{CO_2} + \left(M_{CO_2} - \bar{V}_{CO_2} \rho_w\right) g dz = 0. \tag{8}$$

Equation 8 is the condition for sedimentation–diffusion equilibrium Archibald (1947), Wales et al. (1948), Goldberg (1953), Williams et al. (1958), Mashimo (1988), Rasa et al.

(2005), Fujita (2016), Perrin (2013). The term $\frac{RT}{x_{CO_2}} dx_{CO_2}$ denotes molecular diffusion, driven by the concentration gradients of CO_2 in the aqueous phase. The term $\left(M_{CO_2} - \bar{V}_{CO_2}\rho_w\right) g dz$ denotes the sedimentation effect caused by a centrifugal field (gravity in this case). In fields relevant to geology, the term "sedimentation" typically describes the deposition of particles at the macroscopic level such as sand grains; in a broad sense, sedimentation can occur in solutions of single molecules as well, such as aqueous solutions of protein. In fact, sedimentation–diffusion equilibrium in a centrifugal field has become a well-established method to accurately measure the molecular weight of protein, where the centrifugal field is significantly exaggerated by ultracentrifugation Goldberg (1953), Teller (1973), Cole et al. (2008), Zhao et al. (2013). At the equilibrium state, the concentration profile of dissolved protein becomes non-uniform due to the balance between the sedimentation effect and molecular diffusion.

Many theoretical studies in petroleum reservoirs have shown that on a spatial scale of hundreds of meters, the sedimentation effect of molecules can lead to significant composition variation in hydrocarbon mixture Muskat (1930), Sage and Lacey (1939), Schulte et al. (1980), Whitson et al. (1994), Lira-Galeana et al. (1994), Padua (1999), Espósito et al. (2000), Galliero et al. (2016). In this study, we show mathematically that the sedimentation effect can occur in the aqueous phase with dissolved CO_2 as well, where the CO_2 molecules tend to sink to the bottom of the system.

Therefore, the aqueous phase that is initially out of equilibrium will equilibrate through non-convective transport of dissolved CO_2 driven by the gradient of partial molar free energy. The net flux of dissolved CO_2 can be described by the generalized form of Fick's law, i.e.,

$$J = -\frac{\tau D c_{CO_2}}{RT} \frac{dF^{aq}_{CO_2}}{dz}, \tag{9}$$

where τ is tortuosity for diffusion in porous media, c_{CO_2} is the CO_2 concentration in $\frac{mol}{m^3}$, and J is the CO_2 flux in $\frac{mol}{m^2 s}$. Here, we use $\tau = \phi\left(1 - \bar{S}^{init}_{CO_2}\right)$ to account for the reduced available area open to diffusion, where ϕ is the porosity, $\bar{S}^{init}_{CO_2}$ is the average initial gas saturation. Under isothermal conditions, the system approaches equilibrium by fulfilling Eqs. 1, 2 and 3, and no geothermal gradients are present.

2.1.2 Steady State Under Non-isothermal Condition

When a geothermal gradient is imposed on the system, i.e., $dT \neq 0$, the problem falls into the category of non-equilibrium thermodynamics. The difference compared to an isothermal system is that at the steady state, the entropy of the non-isothermal system continues increasing due to the heat transferred into the system through geothermal gradients (Kempers 1989; Firoozabadi et al. 2000; Firoozabadi 2016; Nikpoor et al. 2016). The condition for the system to approach steady state becomes

$$\frac{d\mu^{aq}_{CO_2}}{dz} + M_{CO_2} g = \frac{\partial \mu^{aq}_{CO_2}}{\partial T} \nabla T, \tag{10}$$

where ∇T is the geothermal gradient. Here, we use the term "steady state" instead of "equilibrium" to describe the state when the flux in the system does not vary with time.

We compare the concentration term and the thermal gradient term in Eq. (4-26.1) in Haase (1968) to obtain an explicit form, i.e.,

$$\left(\frac{\partial \mu_{CO_2}^{aq}}{\partial T}\right)\Big|_{P,x_{CO_2}} dT = R\alpha_T dT, \tag{11}$$

where $\alpha_T = \frac{D_{therm}}{Dx_{CO_2}x_w}$ is defined as thermal diffusion factor, x_w is the water mole fraction, D_{therm} is the thermal diffusion coefficient, and D is the molecular diffusion coefficient. Detailed derivation can be found in Online Resource. Equation 11 indicates that the chemical potential disequilibrium can result from a thermal gradient dT, driving the CO_2 molecules to drift along the direction of the thermal gradient, known as the Soret effect (Kempers 1989, 2001; Platten 2006; Rahman and Saghir 2014). It should be noted that the significance of the Soret effect in CO_2-water systems is still unclear. To the authors' knowledge, there are few experimental studies that measure the thermal diffusion factor α_T in such systems. Therefore, Eq. 11 merely illustrates that chemical potential disequilibrium due to thermal gradients potentially serves as another mass transfer mechanism. In fact, the impact of geothermal gradients is complicated involving multiple processes that can interactive with each other such as density-driven convection Wooding (1957); Donaldson (1962). Complications of non-isothermal systems will be discussed in detail in Sect. 4.1.

2.2 The Role of Residually Trapped Gas in Thermodynamic Potential

When residually trapped CO_2 ganglia coexist with the reservoir brine, we assume that the chemical potential of the dissolved CO_2 is at local equilibrium with the chemical potential of the separate-phase CO_2 in the gas ganglionSuekane et al. (2008), i.e.,

$$\mu_{CO_2}^{aq} = \mu_{CO_2}^{g}, \tag{12}$$

where $\mu_{CO_2}^{g}$ denotes the chemical potential of CO_2 in the gas phase. In other words, the concentration of dissolved CO_2 is at its local solubility, depending on local temperature and the pressure in the adjacent CO_2 ganglia. This local equilibrium assumption suggests that any spatial variation of chemical potential among residually trapped CO_2 ganglia will lead to a chemical potential gradient in dissolved CO_2, inducing non-convective transport of CO_2 in the aqueous phase. For example, variation of capillary pressure among residually trapped gas results in concentration gradients in the aqueous phase, inducing inter-ganglion diffusion to redistribute the mass among residually trapped gas Xu et al. (2017), de Chalendar et al. (2018, 2019), Xu et al. (2019), Li et al. (2020).

In this study, we demonstrate that concentration variations caused by hydrostatic pressure gradients induce non-convective transport. The chemical potential of residually trapped gas $\mu_{CO_2}^{g}(T,P)$ is determined by local temperature T and local gas-phase pressure P, where the gas-phase pressure is $P = P_w + P_c$, the sum of local water pressure P_w and the capillary pressure P_c. As can be seen, the water pressure varies with depth z due to hydrostatic pressure, i.e., $P_w = -\rho_w g z$; under non-isothermal conditions, the temperature $T(z)$ varies with depth as well. Although CO_2 in the two phases reaches equilibrium locally, it is out of global equilibrium due to changes of water pressure and temperature with depth. Therefore, in regions where the two phases coexist, the solubility of dissolved CO_2 will vary with depth, inducing molecular diffusion of dissolved CO_2, thus redistributing the CO_2 until the system approaches an equilibrium or a steady state.

By taking capillary pressure into consideration, we obtain an expression for the local solubility of dissolved CO_2, i.e.,

$$x_{CO_2}(T(z), P(z)) = x_{CO_2,0}\big(T(z), P_w(z)\big) + \frac{P_c\big(S_w\big)}{\frac{dP}{dx_{CO_2}}(z)}, \tag{13}$$

where $x_{CO_2,0}$ is the CO_2 solubility at the local reservoir condition $\big(T, P_w\big)$, S_w is the saturation of the aqueous phase, and $\frac{dP}{dx_{CO_2}}$ is a partition coefficient of CO_2 in the aqueous phase. Under reservoir conditions, the partition coefficient is a strong function of pressure and thus varies with depth Spycher et al. (2003). To accurately calculate CO_2 solubility while reducing computational complexity, we compute one partition coefficient $\frac{dP}{dx_{CO_2}}$ at each reservoir pressure P_w based on CO_2 partition data provided in Spycher et al. (2003). These partition coefficients are then treated as constants for calculating the CO_2 concentration change due to a change of capillary pressure. This approximation is reasonable since the change of capillary pressure is on the order of 10^3 Pa, which is much smaller than the reservoir pressure P_w ($\sim 10^7$ Pa). Eq. 13 shows that the spatial distribution (z) and the capillary pressure $\big(P_c\big)$ of residually trapped CO_2 ganglia determine the strength of molecular diffusion. In turn, molecular diffusion can change the capillary pressure of gas ganglia by redistributing separate-phase CO_2, influencing the driving force for diffusion.

2.3 Relaxation of the Ideal-solution Assumption

As shown in Eq. 3, the direction and magnitude of the sedimentation effect is determined by the partial molar volume of dissolved CO_2, $\bar{V}_{CO_2}$. Partial molar volume of a dissolved substance is defined as the molar volume increase of the solution when adding an infinitesimal amount of the pure substance. It represents the "true" molar volume of the solute accounting for the interaction between components in the solution. In solutions with strong non-ideality, partial molar volume of a substance differs significantly from its molar volume at the pure state. Figure 2a compares the partial molar volume of dissolved CO_2 and the molar volume of pure CO_2 at reservoir conditions. The data are generated by ECO2N, an equation of state specifically designed for applications on geological CO_2 storage in aquifers Pruess and Spycher (2007). ECO2N describes the thermodynamic properties of CO_2-water-NaCl system over a wide range of temperature (10 ^{o}C - 100 ^{o}C), pressure (up to 600 bar) and salinity condition (up to saturated NaCl brine). The fluid properties within this range achieve an excellent agreement with experimental data Spycher et al. (2003); Spycher and Pruess (2005). As can be seen, the molar volume of dissolved CO_2 estimated by ideal solution assumption deviates significantly from its true partial molar volume. The partial molar volume of dissolved CO_2 is approximately constant within the interested pressure and temperature range, since the properties of the aqueous phase seldom vary. Therefore, here we only show the curve for partial molar volume at 50 ^{o}C for better visualization, as other curves within the temperature range 50^{o}C–90^{o}C overlap this curve.

As a result, accurate quantification of the sedimentation effect relies on relaxation of the ideal solution assumption. As we show in Fig. 2b, the ideal-solution assumption leads to a negative CO_2 flux, suggesting that CO_2 would migrate upward under this circumstance. This result is consistent with the conclusion in Xu et al. (2019), which concludes that CO_2 molecules are "buoyant" in the aqueous phase, and thus the gas phase accumulates at the top of the system under ideal solution assumption. However, Fig. 2b also shows that when

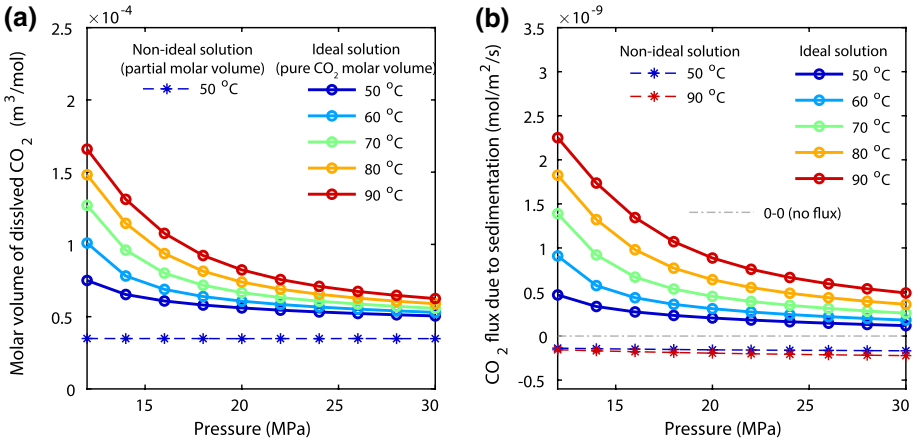

Fig. 2 **a** Comparison between the partial molar volume of dissolved CO_2 and the CO_2 molar volume estimated by ideal solution assumption. The estimation under ideal solution assumption is the molar volume of pure CO_2. The ideal solution assumption leads to overestimation of the molar volume of dissolved CO_2. Here, we only show the curve for partial molar volume at 50 ^{o}C for better visualization, as other curves within the temperature range 50^{o}C - 90^{o}C overlap this curve. **b** Comparison of the CO_2 fluxes in the aqueous phase due to sedimentation, calculated with or without ideal solution assumption. The flux is calculated using Eq. 3 and Eq. 9 by assuming $\tau = 1$ and CO_2 concentration constant. The ideal solution assumption leads to an "upward" CO_2 flux due to sedimentation; while in a more realistic solution accounting for non-ideality, the CO_2 flux due to sedimentation is "downward"

relaxing the ideal solution assumption, the direction of the CO_2 flux due to sedimentation is reversed to positive, and the magnitude of the flux is nearly a constant within the interested range of reservoir conditions. Therefore, the CO_2 flux due to sedimentation is downward, which agrees well with the fact that CO_2 solution is slightly denser than pure water Teng et al. (1997), Garcia (2001), Riaz et al. (2006).

3 Redistribution of Residually Trapped Gas

3.1 Mathematical Formulation of the Gas Redistribution Problem

As shown in Fig. 1, when neglecting any convection in the horizontal direction, the studied system can be reduced to a one-dimensional column of porous medium which initially contains residually trapped CO_2 ganglia and an aqueous phase at local equilibrium with the gas phase. We focus on the redistribution of the gas phase; at the continuum scale, this redistribution is manifested as change of the gas phase saturation. The gas phase is assumed to remain immobile during redistribution such that the only mass transfer mechanism is non-convective transport of dissolved CO_2 in the aqueous phase. The mass balance of CO_2 in this column can be written as

$$\frac{\partial}{\partial t}\left(\frac{\phi S_w \rho_w x_{CO_2}}{M_w} + \frac{\phi S_{CO_2} \rho_{CO_2} y_{CO_2}}{M_{CO_2}}\right) = \frac{\partial J}{\partial z}, \tag{14}$$

where M_w is the molar weight of the aqueous phase, S_{CO_2} is the saturation of separate-phase CO_2, and ρ_{CO_2} is the density of the separate-phase CO_2. The two terms on the left hand side represent the mass of CO_2 in the aqueous phase and in the gaseous phase, respectively. As we show in the previous work Li et al. (2020), the derivative of the first term is small compared to the second term, so that the first term is neglected during our calculation. Detailed explanation can be found in Online Resource. Using Eq. 9 to represent the flux J, the mass balance equation becomes

$$\frac{\partial}{\partial t}\left(\frac{\phi S_{CO_2}\rho_{CO_2}}{M_{CO_2}}\right) = \frac{\partial}{\partial z}\left(-\frac{\tau D c_{CO_2}}{RT}\frac{\partial F^{aq}_{CO_2}}{\partial z}\right), \tag{15}$$

where the gradient of the partial molar free energy is represented by Eq. 3.

The top and bottom boundaries of the system are closed $J(z = 0, L) = 0$, where L is the column height. The initial condition for the system is stable coexistence of residually trapped CO_2 and the aqueous phase throughout the entire column. The initial distribution of residually trapped CO_2 saturation is generated by macroscopic percolation simulation, a reduced-physics approach to accurately quantify both residual trapping and capillary heterogeneity trapping Ni et al. (2021) (see Online Resource for details). The generated gas saturation maps have taken into consideration the impact of capillary heterogeneity and hysteresis. The aqueous phase CO_2 concentration is linked to the gas phase saturation through capillary pressure curves according to Eq. 13. We use a capillary pressure model consistent with our previous study Li et al. (2020), which is shown in detail in Online Resource. The current capillary pressure model is adopted here to represent the following key features of residually trapped gas. First, pore-scale modeling of Ostwald Ripening using conically shaped pore throats by de Chalendar et al. (2018) shows that for pore-filling bubbles, a volume increase will push the bubble interface into local pore throats, leading to an increase of capillary pressure. This trend in capillary pressure for growing bubbles is consistent with the pore-scale analysis by McClure et al. (2016). Second, the capillary pressure of residually trapped gas at the end of imbibition is on the same order of magnitude as the entry pressure of the rock Garing et al. (2017). At a low gas saturation, the capillary pressure of residually trapped gas can vary within this range due to different spatial distribution and connectivity of the gas phase McClure et al. (2016). To date, there are no direct measurements available for the capillary pressure curves of trapped gas ganglia in real rocks during Ostwald Ripening, and future work involving these measurements would be beneficial.

In summary, the system represented by Eq. 15 and the above boundary conditions and initial conditions can be solved numerically to obtain the redistribution process of residually trapped gas phase. The system is solved by an explicit Euler scheme in this study. The physical properties of the example system studied here are representative of a typical carbon sequestration reservoir Krevor et al. (2012); Pini et al. (2012), shown in Online Resource.

3.2 Redistribution of Residually Trapped Gas

3.2.1 The Impact of Hydrostatic Pressure

In regions of the system where the two phases coexist, the dissolved CO_2 concentration is determined by local equilibrium between the two phases. Under isothermal conditions,

CO_2 solubility increases with depth due to hydrostatic pressure, creating a concentration gradient in the aqueous phase. This concentration gradient induces an upward diffusive flux of CO_2. At the same time, the sedimentation effect creates a downward flux of dissolved CO_2. The system approaches steady state when the two fluxes counterbalance each other throughout the column.

Figure 3 shows the redistribution of residually trapped gas in a homogeneous column under isothermal conditions. As can be seen, the CO_2 concentration gradient induces an upward diffusive flux in the aqueous phase to transport CO_2 toward the top of the column. As a result, the gas phase accumulates at the top of the column underneath the seal. The increase in gas saturation under the seal leads to an increase in capillary pressure, raising the local CO_2 concentration at the top of the system (Eq. 13). The gas phase is eventually depleted at the bottom of the column, where the CO_2 concentration drops below local

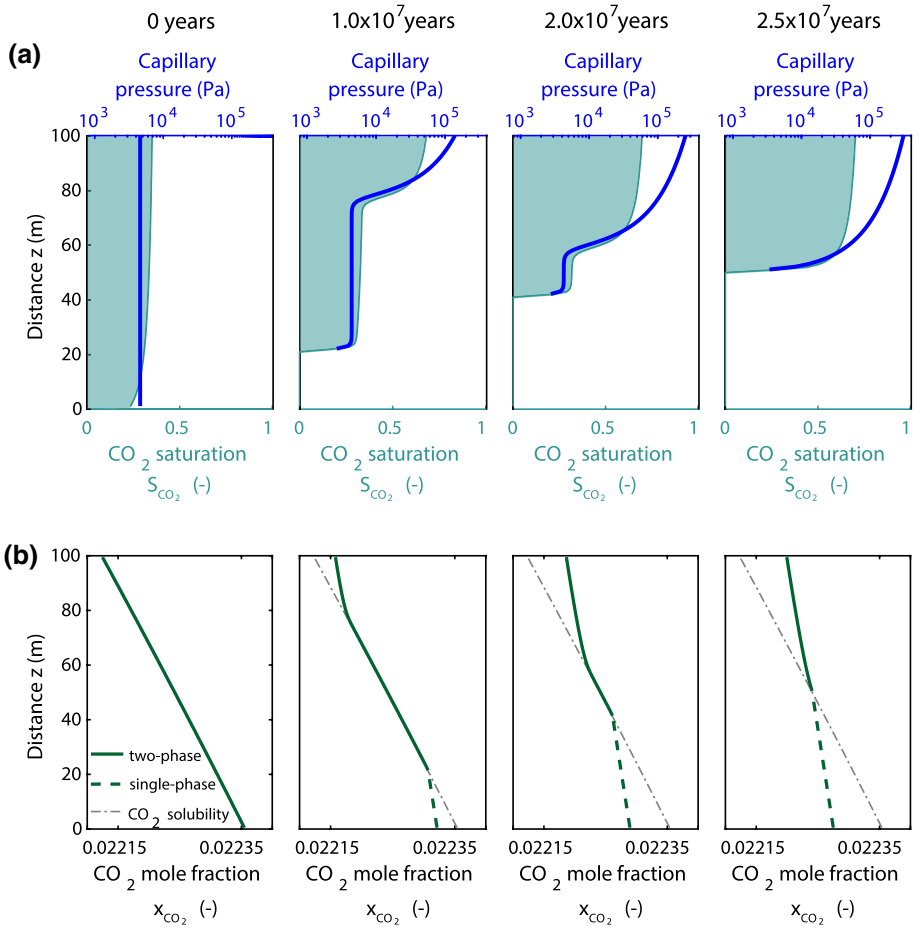

Fig. 3 Redistribution of the gas phase due to non-convective transport in a homogeneous system under isothermal condition. **a** The evolution of the gas phase saturation and the capillary pressure profile during redistribution of the residual gas phase. **b** The evolution of CO_2 concentration profile during redistribution of the residual gas phase. The entry pressure profile and capillary pressure curves can be found in Online Resource

solubility under water pressure. The net concentration gradient decreases with redistribution of the gas phase; at steady state, the concentration gradient counterbalances the sedimentation effect such that the net flux of CO_2 becomes zero. The saturation profile of the gas phase achieves capillary-gravity-sedimentation equilibrium to minimize the CO_2 partial molar free energy gradient in the two-phase zone. Therefore, due to the sedimentation effect, the steady-state CO_2 concentration gradient is nonzero. For the system shown in Fig. 3, the steady state is reached in approximately 2.5×10^7 years.

In this work, we only focus on the non-convective transport and neglected any mobilization of the gas phase. It should be noted that in regions where the gas phase saturation increases, the gas phase is highly likely to become mobile at some point. Although gas-phase mobilization is beyond the scope of this study, characterization of resulting gas mobilization is an interesting topic for future research and is underway as our ongoing study.

3.2.2 The Impact of Capillary Heterogeneity

Evolution of the gas saturation in heterogeneous systems is similar to that for a homogeneous system, but local variations in capillary pressure can temporarily and locally accelerate or counteract the upward flux of CO_2. Figure 4 shows redistribution of the residual gas phase in a heterogeneous system under isothermal conditions. The reservoir conditions are the same as for the homogeneous case shown in Fig. 3. As can be seen, although the CO_2 solubility gradient due to hydrostatic pressure is similar to the homogeneous case, the non-uniform capillary pressure profile imposes additional concentration gradients between layers, initiating local redistribution of the gas phase. Concentration gradients due to capillary heterogeneity are reduced over time, depending on the thickness of the layers and the contrast in rock properties. Eventually, concentration gradients due to hydrostatic pressure regain its dominant role in transporting the gas phase to the top of the column. The steady-state distribution of the gas phase follows capillary-gravity-sedimentation equilibrium similar to the homogeneous case shown in Fig. 3. The overall timescale for the heterogeneous system to reach steady state does not differ significantly from that for the homogeneous case, due to the same dominant driving force.

It should be noted that the main assumption here is that the gas phase remains immobile during the entire course of evolution. In one-dimensional systems considered here, migration of the gas is limited in the vertical direction; mobilization of the gas phase in two-dimensional models may induce convective flow and thus potentially change the behavior of gas redistribution. This is an interesting topic and is currently undertaken as our ongoing study.

3.2.3 The Impact of Geothermal Gradients

Figure 5 compares the steady state of residual gas redistribution in a non-isothermal case with a geothermal gradient of 25 ^{o}C/km with the isothermal case shown in Fig. 3. The properties other than the geothermal gradient are the same in both cases. As shown in Fig. 5 a, c and e, the timescale for equilibration is ten times longer in the non-isothermal cases. Although the two cases exhibit a similar pattern during saturation evolution, and the steady-state distribution of the gas phase in both cases follows capillary-gravity-sedimentation equilibrium, comparison of Fig. 5b and d shows that the initial CO_2 concentration

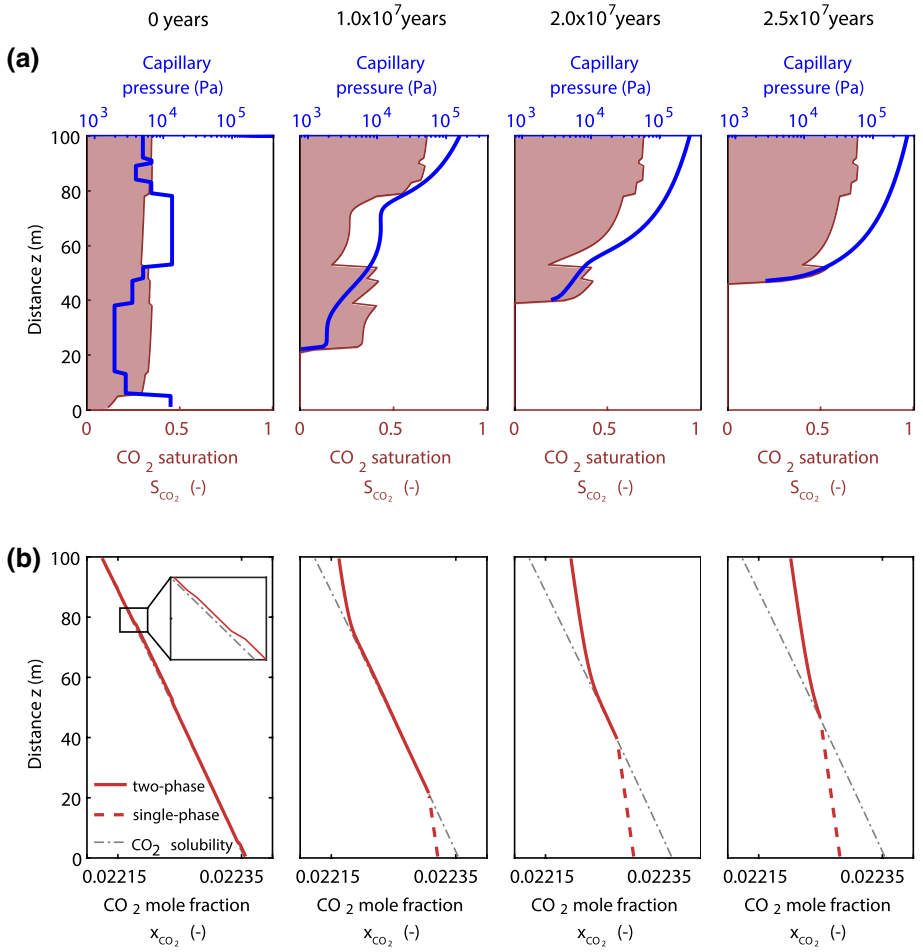

Fig. 4 Redistribution of the gas phase due to non-convective transport in a heterogeneous system under isothermal condition. **a** The evolution of the gas phase saturation and the capillary pressure profile during redistribution of the residual gas phase. **b** The evolution of CO_2 concentration profile during redistribution of the residual gas phase. The entry pressure profile and capillary pressure curves can be found in Online Resource

gradient in the aqueous phase is 50% smaller than in the isothermal case. The redistribution process is decelerated by this reduced driving force due to the geothermal gradient.

The reduction of CO_2 solubility gradient originates from the opposite dependence of solubility on pressure and temperature. When the geothermal gradient is sufficiently large, the solubility at the top will eventually exceed that at the bottom, altering the direction of the solubility gradient. In this case, the net flux of non-convective transport of CO_2 becomes downward, causing the gas phase to accumulate in the lower portion of the system. For the reservoir condition given in the example case in Fig. 3 (75 ^{o}C and 25 MPa), the geothermal gradient sufficient to reverse the CO_2 solubility gradient is 40^{o}C/km. In a shallower reservoir, the required geothermal gradient could be smaller. See Online Resource for details.

However, in a realistic scenario where the mobilization of the gas phase is taken into consideration, the gas phase is highly likely to become mobile when its saturation

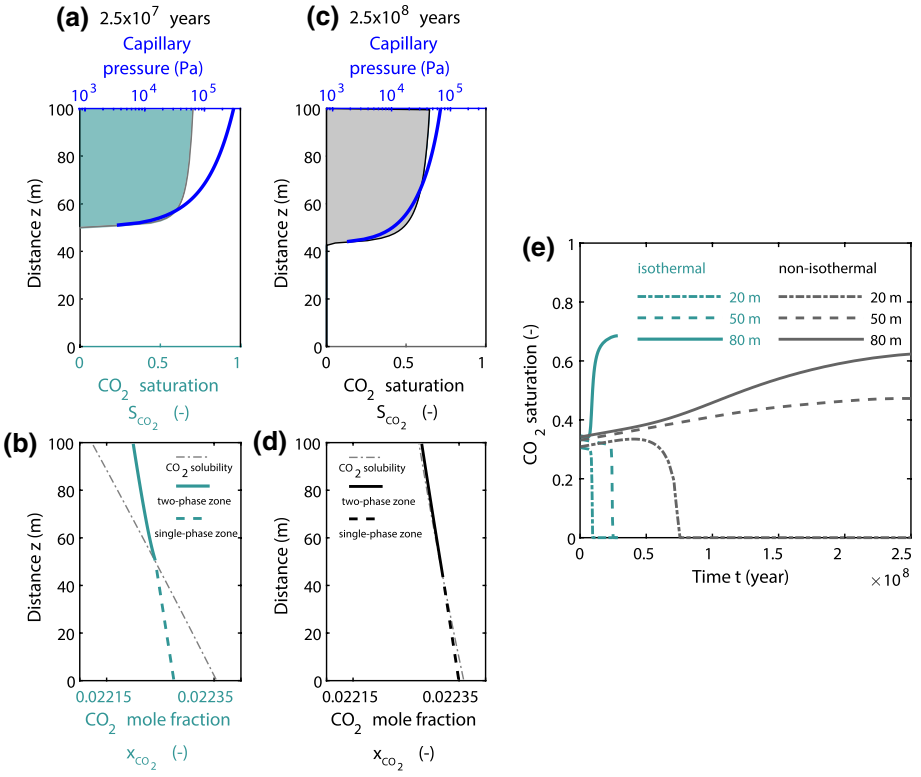

Fig. 5 **a** Steady-state saturation distribution and **b** steady-state CO_2 mole fraction in the aqueous phase of the homogeneous, isothermal case shown in Fig. 3. **c** Steady-state saturation distribution and **d** steady-state CO_2 mole fraction in the aqueous phase of a homogeneous, non-isothermal case with a geothermal gradient of 25^{o}C. Other parameters of the non-isothermal case are the same as the isothermal case. **e** Evolution of CO_2 saturation at different elevations in both the isothermal case and the non-isothermal case. Redistribution of the gas phase exhibits the same pattern in both cases; however, the time scale of redistribution in the non-isothermal case is 10 times longer since the geothermal gradient reduces the CO_2 concentration gradient in the aqueous phase

increases. At some point, the gas phase accumulating in the lower portion would flow back to the top due to buoyancy forces. Nonetheless, a geothermal gradient can mitigate the upward diffusive flux and thus can delay the upward migration of the gas phase.

3.3 Comparison of Non-convective Fluxes

Figure 6 compares the direction and magnitude of the driving forces for molecular diffusion and sedimentation. As can be seen, non-convective transport under isothermal condition is dominated by molecular diffusion driven by CO_2 solubility gradients due to hydrostatic pressure. Under typical reservoir conditions for CO_2 sequestration, the net driving force under isothermal condition is negative to create an upward net flux, causing the gas phase to accumulate in the upper portion of the system. The upward net flux decreases as the depth of the reservoir increases. In non-isothermal system, the upward net flux of CO_2 decreases or even reverses downward due to a geothermal gradient. Therefore, a

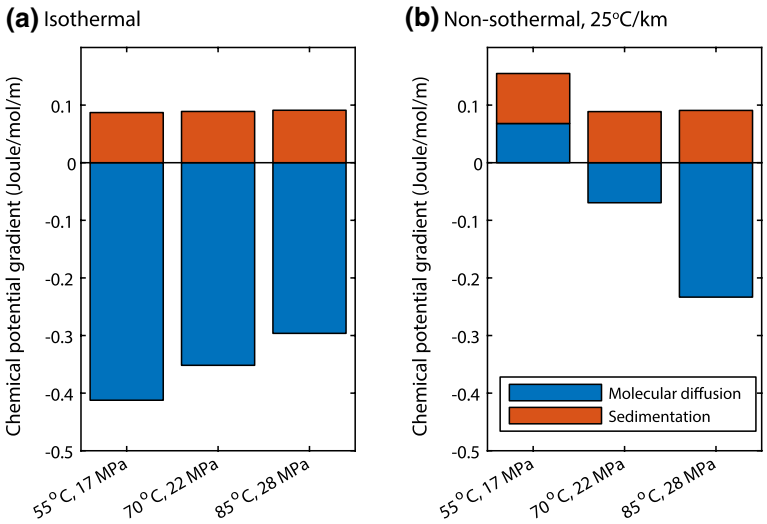

Fig. 6 Comparison of the driving forces for molecular diffusion and the sedimentation effect at different reservoir conditions under **a** isothermal conditions and **b** non-isothermal conditions. The net flux of non-convective transport is upward under isothermal conditions, dominated by molecular diffusion due to CO_2 solubility gradient; however, geothermal gradients can reduce or even reverse the net flux

geothermal gradient can mitigate this upward migration of trapped gas by reducing the contribution of molecular diffusion by decreasing the solubility gradient. The impact of the Soret effect is not included in this section due to its high uncertainty involving lack of experimental data and complex molecular interactions. Detailed discussion on complexity of the Soret effect is shown in Sect. 4.1.

On the other hand, the flux due to the sedimentation effect remains nearly constant due to negligible variation in CO_2 partial molar volume under reservoir conditions relevant to CO_2 sequestration. Under isothermal conditions, the impact of sedimentation effect is small compared to molecular diffusion. The flux due to the sedimentation effect is downward, forming a counter-flux to balance molecular diffusion due to CO_2 solubility gradient. In a recent study exploring the impact of sedimentation on gas-phase redistribution Xu et al. (2019), the authors adopted the ideal-solution assumption by using the molar volume of pure CO_2 to replace its partial molar volume. They therefore concluded that the CO_2 flux due to sedimentation is upward, causing the gas phase to accumulate in the upper portion of the system. As we show in Figs. 2 and 6, in reality, the ideal-solution assumption is a poor predictor of the partial molar volume for the CO_2/water system at reservoir pressure and temperatures, and in fact, the sedimentation is downward.

4 Significance of Residual Gas Redistribution Due to Non-convective Transport

4.1 Complexities Under Non-isothermal Conditions

In addition to molecular diffusion and the sedimentation effect, non-isothermal systems may induce an additional flux of non-convective transport as shown in Eq. 10, which describes the mass flux of CO_2 induced by the geothermal gradient $dT \neq 0$. This phenomenon, also known as the Soret effect, occurs when a non-uniform temperature profile feeds energy into the system, which creates a heat flow that can separate different species in the aqueous phase Haase (1968); Garriga et al. (2002); Groot and Mazur (2013); Eslamian (2012). According to Eq. 11, the driving force for diffusion due to the Soret effect is co-determined by the geothermal gradient ∇T and the thermal diffusion factor α_T. The characteristics of non-convective transport due to the Soret effect relies on accurate measurement of the value of α_T.

To our knowledge, no experimental data are currently available on α_T in water-CO_2 systems. One approach to determine α_T is to perform Monte Carlo molecular simulation of water-CO_2 systems, which is beyond the scope of this study. Most available experimental measurements of α_T focus on hydrocarbon fluids, aqueous solutions of alcohols and polymers Emery and Drickamer (1955), Tichacek et al. (1956), Shukla and Firoozabadi (1998), Ning and Wiegand (2006), Stadelmaier and Kohler (2009), Eslamian (2012), which can seldom be directly generalized to water-CO_2 systems. Both the sign and magnitude of α_T differ significantly from mixture to mixture due to complex molecular-level interactions between species. For reference, α_T in water–ethanol systems at 25 ^{o}C ranges from -0.5 to +0.29, and α_T in water–methanol systems at 40 ^{o}C ranges from -0.46 to 1.17 Tichacek et al. (1956).

In fact, solute transport in non-isothermal systems can become extremely complicated due to coexistence of other processes, such as convective flow due to Rayleigh–Benard instability. In this case, the assumption of non-convection used in this study needs to be relaxed. The impact of geothermal gradients on solute transport and redistribution of residually trapped CO_2 remains an interesting topic for future study. Nonetheless, geothermal gradients can significantly reduce the rate at which trapped CO_2 accumulates underneath a seal.

4.2 Timescales for Residual Gas Redistribution

To quantify the timescale for residual gas redistribution due to non-convective transport, here we develop the concept of the "gas depletion rate." As can be seen in Figs. 3, 4 and 5, the gas phase begins to be depleted from the bottom of the system, forming a gas-depleted zone containing only the aqueous phase. Figure 7a tracks the temporal location of the boundary between the gas-depleted zone and the two-phase zone. As can be seen, the boundary moves at an approximately constant speed before reaching equilibrium. In the heterogeneous case, the velocity of the boundary fluctuates weakly due to capillary heterogeneity, while the overall velocity remains similar to that for the homogeneous case. This result serves as additional evidence that capillary heterogeneity has a local rather than global effect on the system.

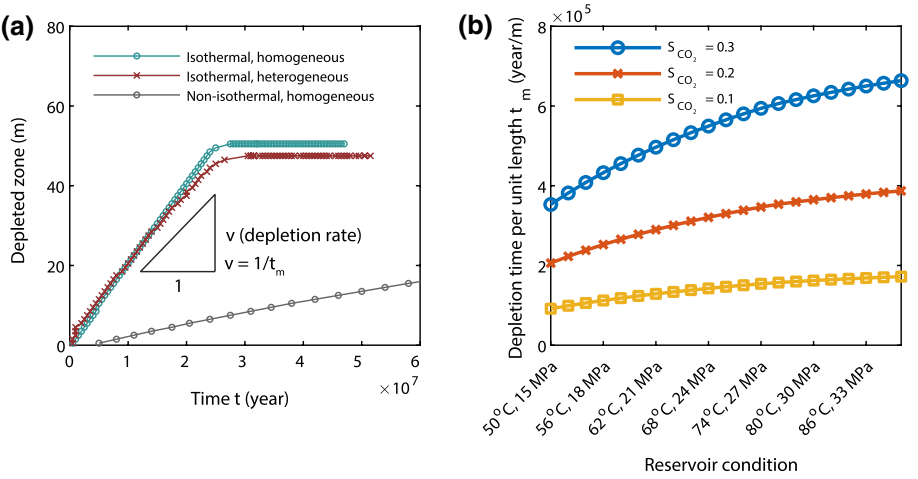

Fig. 7 **a** The temporal elevation of the boundary between the gas-depleted zone and the two-phase zone during redistribution of residual gas. The cases shown here correspond to cases in Figs. 3, 4 and 5. **b** Depletion time per unit length $t_m = \frac{1}{v}$ under different reservoir conditions. All the data points are under isothermal conditions. Depletion time for three different values of average initial gas saturation is shown here, suggesting that the timescale for gas redistribution also depends on the total amount of residually trapped gas in addition to reservoir condition. Within reservoir conditions relevant to CO_2 storage, the timescale is on the order of hundreds of thousands years per meter of upward migration

The slope of the line in Fig. 7a is the velocity of the boundary of the gas-depleted zone v, which can be obtained by combining and Eq. 9 and 15. We substitute $\rho_{CO_2}\bar{S}^{init}_{CO_2}\phi$ for m_{CO_2}, which is the average amount of CO_2 in the gas phase initially in place. Therefore, the velocity of the boundary v when it moves to location z can be estimated by:

$$v = \frac{J}{m_{CO_2}} = -\frac{\tau D c_{CO_2}}{\phi \rho_{CO_2} \bar{S}^{init}_{CO_2} RT} \frac{d\mu}{dz}. \tag{16}$$

The time required to deplete the gas phase in a unit length is simply the inverse of the depletion rate, i.e., $t_m = \frac{1}{v}$. This depletion time can be used as a characteristic time to measure the timescale of gas redistribution. Figure 7b shows the depletion time under different reservoir conditions relevant to CO_2 sequestration. As can be seen, both reservoir conditions and saturation of residually trapped gas can determine the timescale of gas redistribution by determining the magnitude of driving forces and the total amount of gas. Under isothermal conditions, the timescale for residual gas redistribution is on the order of 10^5 years per meter. This time scale agrees well with the cases reported in Figs. 3 and 4, where the depletion time per unit length is approximately 5×10^5 years per meter. For a typical CO_2 sequestration reservoir shown in Figs. 3 and 4 with a 50-meter-thick gas-depleted zone, one can expect that the gas redistribution will approach equilibrium in 25 million years. This extended time period suggests that gas redistribution due to non-convective transport is extremely slow such that the residually trapped gas can remain stably trapped for millions of years.

A study on the impact of gravity-induced flux on gas redistribution Xu et al. (2019) reported a gas depletion rate on the order of thousands of years per meter in a demonstrative case, which is ten times faster than the rate we predict. Three factors explain the order

of magnitude differences between our results. First, the transport mechanisms investigated in these two studies are different. In our study, the transport mechanism is a combination of molecular diffusion due to hydrostatic gradients and a downward sedimentation effect due to gravity in a non-ideal solution, while Xu et al. (2019) studied an upward sedimentation effect in an ideal-solution setting. Second, the model in Xu et al. (2019) is calculated for a very shallow and high-temperature CO_2 storage reservoir (10 MPa and 60 ^{o}C), where the CO_2 density is 325 kg/m^3. Under these conditions, the driving forces for non-convective transport are much higher than would be expected for a typical CO_2 storage reservoir such as that used in our calculations (25 MPa and 75 ^{o}C, 717 kg/m^3). The low density of the gas phase contains less CO_2, which also contributes to accelerating the gas phase redistribution. Third, their hypothetical pore geometry for demonstrative purposes accelerates gas redistribution as a secondary factor. In our work, the model is based on actual properties of a Berea sandstone, which is a commonly used analogue for CO_2 storage studies Krevor et al. (2012), and more realistic pressure and temperature for CO_2 storage, leading to a larger timescale for gas redistribution. The time scale derived from our model is representative of realistic scenarios for CO_2 storage.

4.3 Comparison Between Timescales of Convective and Non-convective Transport

Dissolution of CO_2 due to convective mixing is another mechanism affecting the long-term fate of stored CO_2Bourg et al. (2015). While non-convective transport mechanisms lead to accumulation at the top of the storage reservoir, convective mixing can gradually reduce the CO_2 accumulated under the seal. Therefore, comparison between the timescales of the two competing mechanisms is relevant to long-term security of CO_2 storage. The characteristics and timescales of convective mixing vary significantly at different stages of the process. There exist various methods to decompose convective mixing into multiple flow regimes Emami-Meybodi et al. (2015). Here for simplicity, we pick three time points to mark the beginning, the middle and the late stage of convective mixing as characteristic times, which are the onset of instability, end of early convection Hassanzadeh et al. (2007) and convective shutdown-Hewitt et al. (2013), respectively.

Figure 8 shows the timescale comparison between convective mixing and gas-phase redistribution due to non-convective transport. Here, the progress of convective mixing is characterized by the above three time points, where the parameters used in these calculations include reservoir thickness $H = 100$ m, temperature $T = 75\ ^{o}$C, brine density difference $\Delta\rho = 10$ kg/m^3, water viscosity $\mu_w = 3.8 \times 10^{-4}$ Pa s, diffusion coefficient $D = 5 \times 10^{-9}$ m^2/s and porosity $\rho = 0.2$. Two examples of CO_2 storage projects are shown on the same plot Bickle et al. (2007), Strandli (2015). As can be seen, the timescales of convective mixing and non-convective mixing are approximately the same order of magnitude in reservoirs with low permeability ($k < 10$ mD). In reservoirs with higher permeability ($k > 10$ mD) such as the Illinois basin and Sleipner, convective mixing is orders of magnitude faster than non-convective transport. Only after the convection shuts down will non-convective transport dominate redistribution of dissolved CO_2.

5 Implications for Geological Gas Migration and Conclusions

This study demonstrates that non-convective transport through the aqueous phase will redistribute residually trapped gas, driven by disequilibrium of partial molar free energy potentials. From the perspective of geological storage of CO_2, residually trapped gas is

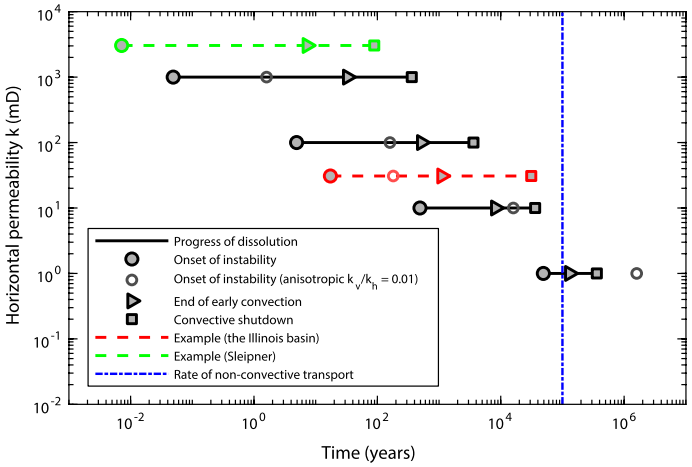

Fig. 8 Timescale comparison between CO_2 dissolution due to convective mixing and CO_2 redistribution due to non-convective transport. Three key characteristic times are adopted here to describe the progress of dissolution, including onset of instability, end of early convectionHassanzadeh et al. (2007) and convective shutdownHewitt et al. (2013). The parameters used in these calculations include reservoir thickness $H = 100$ m, temperature $T = 75$ °C, brine density difference $\Delta\rho = 10$ kg/m^3, water viscosity $\mu_w = 3.8 \times 10^{-4}$ Pa s, diffusion coefficient $D = 5 \times 10^{-9}$ m^2/s and porosity $\phi = 0.2$

expected to be redistributed in the storage reservoir at a rate of approximately 10^5 years per meter. This extremely slow redistribution rate suggests that residually trapped CO_2 will remain immobilized for over many hundreds of thousands of years when no convective flow of the gas phase is considered. However, during redistribution of the gas phase, in some portions of the reservoir, CO_2 saturations will increase, causing remobilization of the trapped gas. This could accelerate the accumulation of CO_2 underneath the seal.

The mechanisms for gas migration studied in this work may also contribute to secondary basin-scale migration of natural gas. Secondary migration refers to the movement of natural gas in a porous reservoir toward the trap after leaving the organic-rich source rock Schowalter (1979). A widely accepted theory of secondary migration states that the natural gas moves updip in the form of a continuous phase driven by buoyancy, leaving "residual stains" along the migration pathways. Although a residual gas trapping along the migration pathways has been demonstrated in laboratory experiments Horseman et al. (1999), little field evidence for residual gas is evident in core samples taken along possible gas migration pathways. The lack of evidence for residually trapped gas is rationalized by the hypothesis that gas only migrates in a meter-thick layer below the dipping seal and whatever residual gas is left behind is dissolved and diluted by formation water Schowalter (1979); McAuliffe (1979). Gas redistribution due to the diffusion processes discussed in this work may also contribute to the absence of the residual gas along natural gas migration pathways. In addition to diffusing into the formation water, gas-phase redistribution may aggregate the disconnected residual gas, which may re-initiate convective flow for the trapped gas phase at some point. Considering that the timescale for the diffusion-induced gas redistribution is relatively short compared to the geological timescale for natural gas migration, this new mechanism could potentially accelerate secondary migration of natural gas.

To summarize, this study quantifies redistribution of residually trapped gas due to non-convective transport from a fundamental perspective. Non-convective transport of

residually trapped gas results from the thermodynamic potential disequilibrium due to hydrostatic pressure, geothermal gradients and capillary heterogeneity. The mechanisms of resulting mass transfer include molecular diffusion, the sedimentation effect and potentially the Soret effect. Mathematical modeling shows that molecular diffusion induced by hydrostatic pressure dominates the gas-phase redistribution by transporting CO_2 upward. Eventually, the gas phase accumulates under the seal. The timescale for redistribution under isothermal conditions is on the order of 10^5 years per meter of upward migration at the reservoir scale. Geothermal gradients can somewhat mitigate the accumulation of the gas phase by reducing the solubility gradient of dissolved CO_2. In addition, geological heterogeneity leads to faster non-convective redistribution at a local scale, but in the long run, concentration gradients caused by the hydrostatic pressure gradient dominate the long-term redistribution of CO_2. It is shown that the residually trapped gas phase could remain trapped over an extended time period when no convective flow of the gas phase is considered. However, accumulation of the gas phase due to capillary heterogeneity may remobilize some of the trapped CO_2 and thus significantly accelerate the redistribution process.

Supplementary Information The online version contains supplementary material available at https://doi.org/10.1007/s11242-021-01722-y.Supplementary Information The online version contains supplementary material available at https://doi.org/10.1007/s11242-021-01722-y.

Funding This study was funded by the Global Climate and Energy Project (GCEP), the Stanford Center for Carbon Storage (SCCS), and the Center of Nanoscale Controls on Geologic CO2 (NCGC) funded by the U.S. Department of Energy, under contract number DE-AC02-05CH11231.

Data Availability This study focuses on developing a generalizable, conceptual model; therefore, no field data is used. All parameters used for the conceptual model are listed in the Online Resource with relevant references.

Code Availability Not applicable.

Declarations

Conflicts of interest The authors acknowledge no conflicting financial support for this work.

References

Archibald, W.: A demonstration of some new methods of determining molecular weights from the data of the ultracentrifuge. J. Phys. Chem. **51**(5), 1204–1214 (1947)

Bickle, M., Chadwick, A., Huppert, H.E., Hallworth, M., Lyle, S.: Modelling carbon dioxide accumulation at sleipner: implications for underground carbon storage. Earth Planet. Sci. Lett. **255**(1–2), 164–176 (2007)

Bourg, I.C., Beckingham, L.E., DePaolo, D.J.: The nanoscale basis of co2 trapping for geologic storage. Environ. Sci Technol. **49**(17), 10265–10284 (2015)

Burnside, N., Naylor, M.: Review and implications of relative permeability of co2/brine systems and residual trapping of co2. Int. J. Greenh. Gas Control **23**, 1–11 (2014)

de Chalendar, J.A., Garing, C., Benson, S.M.: Pore-scale modelling of ostwald ripening. J. Fluid Mech. **835**, 363–392 (2018)

de Chalendar, J.A., Garing, C., Benson, S.M.: Pore-scale modelling of ostwald ripening-corrigendum. J. Fluid Mech. **866**, 929–929 (2019)

Chatzis, I., Morrow, N.R., Lim, H.T., et al.: Magnitude and detailed structure of residual oil saturation. Soc. Pet. Eng. J. **23**(02), 311–326 (1983)

Claypool, G.E., Kaplan, I.: The origin and distribution of methane in marine sediments Natural gases in marine sediments, pp. 99–139. Springer, Berlin (1974)

Cole, J.L., Lary, J.W., Moody, T.P., Laue, T.M.: Analytical ultracentrifugation: sedimentation velocity and sedimentation equilibrium. Methods Cell. Biol. **84**, 143–179 (2008)
De Groot, S.R., Mazur, P.: Non-equilibrium thermodynamics. Courier Corporation, USA (2013)
Donaldson, I.: Temperature gradients in the upper layers of the earth's crust due to convective water flows. J. Geophys. Res. **67**(9), 3449–3459 (1962)
Emami-Meybodi, H., Hassanzadeh, H., Green, C.P., Ennis-King, J.: Convective dissolution of co2 in saline aquifers: progress in modeling and experiments. Int. J. Greenh. Gas Control **40**, 238–266 (2015)
Emery, A., Jr., Drickamer, H.: Thermal diffusion in polymer solutions. J. Chem. Phys. **23**(12), 2252–2257 (1955)
Ennis-King, J., Paterson, L., et al.: Role of convective mixing in the long-term storage of carbon dioxide in deep saline formations. In: SPE annual technical conference and exhibition, Society of Petroleum Engineers (2003)
Ennis-King, J., Preston, I., Paterson, L.: Onset of convection in anisotropic porous media subject to a rapid change in boundary conditions. Phys. Fluids **17**(8), 084107 (2005)
Eslamian, M.: Advances in thermodiffusion and thermophoresis (soret effect) in liquid mixtures. Frontiers in Heat and Mass Transfer (FHMT) **2**(4) (2012)
Espósito, R.O., Castier, M., Tavares, F.W.: Calculations of thermodynamic equilibrium in systems subject to gravitational fields. Chem. Eng. Sci. **55**(17), 3495–3504 (2000)
Firoozabadi, A.: Thermodynamics and applications in hydrocarbon energy production. McGraw-Hill Education, USA (2016)
Firoozabadi, A., Ghorayeb, K., Shukla, K.: Theoretical model of thermal diffusion factors in multicomponent mixtures. AIChE J. **46**(5), 892–900 (2000)
Fujita, H.: Mathematical theory of sedimentation analysis. Elsevier, Berlin (2016)
Galliero, G., Bataller, H., Croccolo, F., Vermorel, R., Artola, P.A., Rousseau, B., Vesovic, V., Bou-Ali, M., De Zárate, J.M.O., Xu, S., et al.: Impact of thermodiffusion on the initial vertical distribution of species in hydrocarbon reservoirs. Microgravity Sci. Technol. **28**(2), 79–86 (2016)
Garcia, J.E.: Density of aqueous solutions of co2. Tech. rep., Lawrence Berkeley National Lab.(LBNL), Berkeley, CA (United States) (2001)
Garing, C., de Chalendar, J.A., Voltolini, M., Ajo-Franklin, J.B., Benson, S.M.: Pore-scale capillary pressure analysis using multi-scale x-ray micromotography. Adv. Water Resour. **104**, 223–241 (2017)
Garriga, A., Kurchan, J., Ritort, F.: Strong soret effect in one dimension. J. Statist. Phys. **106**(1–2), 109–123 (2002)
Goldberg, R.J.: Sedimentation in the ultracentrifuge. J. Phys. Chem. **57**(2), 194–202 (1953)
Goldobin, D.S., Brilliantov, N.V.: Diffusive counter dispersion of mass in bubbly media. Phys. Rev. E **84**(5), 056328 (2011)
Haase, R.: Thermodynamics of irreversible processes. Addison-Wesley, Boston (1968)
Hassanzadeh, H., Pooladi-Darvish, M., Keith, D.W.: Scaling behavior of convective mixing, with application to geological storage of co2. AIChE J. **53**(5), 1121–1131 (2007)
Hesse, M., Tchelepi, H.A., Orr, F.M., et al.: Scaling analysis of the migration of co2 in saline aquifers. In: SPE Annual Technical Conference and Exhibition, Society of Petroleum Engineers (2006)
Hewitt, D.R., Neufeld, J.A., Lister, J.R.: Convective shutdown in a porous medium at high rayleigh number. J. Fluid Mech. **719**, 551–586 (2013)
Horseman, S., Harrington, J., Sellin, P.: Gas migration in clay barriers. Eng. Geol. **54**(1–2), 139–149 (1999)
Iglauer, S., Paluszny, A., Pentland, C.H., Blunt, M.J.: Residual co2 imaged with x-ray micro-tomography. Geophysical Research Letters **38**(21), 0094–8276 (2011). https://doi.org/10.1029/2011GL049680
Jiang, F., Tsuji, T.: Impact of interfacial tension on residual co2 clusters in porous sandstone. Water Resour. Res. **51**(3), 1710–1722 (2015)
Juanes, R., Spiteri, E., Orr, Jr F., Blunt, M. J.: Impact of relative permeability hysteresis on geological co2 storage. Water Resour. Res. **42**(12), 0043–1397 (2006). https://doi.org/10.1029/2005WR004806
Kempers, L.: A comprehensive thermodynamic theory of the soret effect in a multicomponent gas, liquid, or solid. J. Chem. Phys. **115**(14), 6330–6341 (2001)
Kempers, L.J.: A thermodynamic theory of the soret effect in a multicomponent liquid. J. Chem. Phys. **90**(11), 6541–6548 (1989)
Krevor, S.C.M., Pini, R., Zuo, L., Benson, S.M.: Relative permeability and trapping of co2 and water in sandstone rocks at reservoir conditions. Water Resour. Res. **48**(2) (2012). https://doi.org/10.1029/2011WR010859
Kumar, A., Noh, M., Pope, G., Sepehrnoori, K., Bryant, S., Lake, L., et al.: Reservoir simulation of co2 storage in deep saline aquifers. In: SPE/DOE Symposium on Improved Oil Recovery, Society of Petroleum Engineers (2004)

Kumar, A., Noh, M.H., Ozah, R.C., Pope, G.A., Bryant, S.L., Sepehrnoori, K., Lake, L.W., et al.: Reservoir simulation of co 2 storage in aquifers. Spe J. **10**(03), 336–348 (2005)
Lei, L., Seol, Y.: Pore-scale investigation of methane hydrate-bearing sediments under triaxial condition. Geophys. Res. Lett. **47**(5), e2019GL086 (2020). https://doi.org/10.1029/2019GL086448
Li, Y., Garing, C., Benson, S.M.: A continuum-scale representation of ostwald ripening in heterogeneous porous media. *Journal of Fluid Mechanics* 889 (2020). https://doi.org/10.1017/jfm.2020.53
Lira-Galeana, C., Firoozabadi, A., Prausnitz, J.M.: Computation of compositional grading in hydrocarbon reservoirs application of continuous thermodynamics. Fluid Phase Equilibria **102**(2), 143–158 (1994)
Mashimo, T.: Self-consistent approach to the diffusion induced by a centrifugal field in condensed matter: sedimentation. Phys. Rev. A **38**(8), 4149 (1988)
McAuliffe, C.D.: Oil and gas migration-chemical and physical constraints. AAPG Bullet. **63**(5), 761–781 (1979)
McClure, J.E., Berrill, M.A., Gray, W.G., Miller, C.T.: Influence of phase connectivity on the relationship among capillary pressure fluid saturation and interfacial area in two-fluid-phase porous medium systems. Phys. Rev. E **94**(3), 033102 (2016)
Mo, S., Zweigel, P., Lindeberg, E.G., Akervoll, I., et al.: Effect of geologic parameters on co2 storage in deep saline aquifers. In: SPE Europec/EAGE Annual Conference, Society of Petroleum Engineers (2005). https://doi.org/10.2118/93952-MS
Muskat, M.: Distribution of non-reacting fluids in the gravitational field. Phys. Rev. **35**(11), 1384 (1930)
Neufeld, J.A., Hesse, M.A., Riaz, A., Hallworth, M.A., Tchelepi, H.A., Huppert, H.E.: Convective dissolution of carbon dioxide in saline aquifers. Geophysical Res. Lett. **37**(22) (2010). https://doi.org/10.1029/2010GL044728
Ni, H., Møyner, O., Kurtev, K.D., Benson, S.M.: Quantifying co2 capillary heterogeneity trapping through macroscopic percolation simulation. Adv. Water Resour. **155**(103), 990 (2021)
Nikpoor, M.H., Dejam, M., Chen, Z., Clarke, M.: Chemical-gravity-thermal diffusion equilibrium in two-phase non-isothermal petroleum reservoirs. Energy Fuels **30**(3), 2021–2034 (2016)
Ning, H., Wiegand, S.: Experimental investigation of the soret effect in acetone/water and dimethylsulfoxide/water mixtures. J Chem Phys. **125** (22), 221102 (2006). https://doi.org/10.1063/1.2402159
Padua, K.: Nonisothermal gravitational equilibrium model. SPE Reserv. Eval. Eng. **2**(2), 211–217 (1999)
Peng, C., Crawshaw, J.P., Maitland, G.C., Trusler, J.M., Vega-Maza, D.: The ph of co2-saturated water at temperatures between 308 k and 423 k at pressures up to 15 mpa. J. Supercrit. Fluids **82**, 129–137 (2013)
Pentland, C., El-Maghraby, R., Georgiadis, A., Iglauer, S., Blunt, M.: Immiscible displacements and capillary trapping in co2 storage. Energy Procedia **4**, 4969–4976 (2011)
Perrin, J.: Brownian movement and molecular reality. Courier Corporation, USA (2013)
Pini, R., Krevor, S.C., Benson, S.M.: Capillary pressure and heterogeneity for the co2/water system in sandstone rocks at reservoir conditions. Adv. Water Resour. **38**, 48–59 (2012)
Platten, J.K.: The soret effect: a review of recent experimental results. J. Appl. Mech. **73**(1), 5–15 (2006). https://doi.org/10.1115/1.1992517
Pruess, K., Spycher, N.: Eco2n-a fluid property module for the tough2 code for studies of co2 storage in saline aquifers. Energy Convers. Manag. **48**(6), 1761–1767 (2007)
Rahman, M., Saghir, M.: Thermodiffusion or soret effect: historical review. Int. J. Heat Mass Transf. **73**, 693–705 (2014)
Rasa, M., Erné, B., Zoetekouw, B., van Roij, R., Philipse, A.: Macroscopic electric field and osmotic pressure in ultracentrifugal sedimentation-diffusion equilibria of charged colloids. J. Phys.: Condensed Matter **17**(15), 2293 (2005)
Riaz, A., Hesse, M., Tchelepi, H., Orr, F.: Onset of convection in a gravitationally unstable diffusive boundary layer in porous media. J. Fluid Mech. **548**(1), 87–111 (2006)
Roof, J., et al.: Snap-off of oil droplets in water-wet pores. Soc. Petrol. Eng. J. **10**(01), 85–90 (1970)
Sage, B.H., Lacey, W.N.: Gravitational concentration gradients in static columns of hydrocarbon fluids. Trans. AIME **132**(01), 120–131 (1939)
Schowalter, T.T.: Mechanics of secondary hydrocarbon migration and entrapment. AAPG Bullet. **63**(5), 723–760 (1979)
Schulte, A, et al.: Compositional variations within a hydrocarbon column due to gravity. In: SPE annual technical conference and exhibition, Society of Petroleum Engineers (1980)
Shukla, K., Firoozabadi, A.: A new model of thermal diffusion coefficients in binary hydrocarbon mixtures. Ind. Eng. Chem. Res. **37**(8), 3331–3342 (1998)
Spycher, N., Pruess, K.: Co2-h2o mixtures in the geological sequestration of co2 ii partitioning in chloride brines at 12–100 c and up to 600 bar. Geochimica et Cosmochimica Acta **69**(13), 3309–3320 (2005)

Spycher, N., Pruess, K., Ennis-King, J.: Co2-h2o mixtures in the geological sequestration of co2 i assessment and calculation of mutual solubilities from 12 to 100 c and up to 600 bar. Geochimica et cosmochimica acta **67**(16), 3015–3031 (2003)
Stadelmaier, D., Kohler, W.: Thermal diffusion of dilute polymer solutions: the role of chain flexibility and the effective segment size. Macromolecules **42**(22), 9147–9152 (2009)
Strandli, C.W.: Multilevel pressure measurements for monitoring and prediction of CO 2 and displaced brine migration. Stanford University, USA (2015)
Suekane, T., Nobuso, T., Hirai, S., Kiyota, M.: Geological storage of carbon dioxide by residual gas and solubility trapping. Int. J. Greenh. Gas Control **2**(1), 58–64 (2008)
Teller, D.C.: [14] characterization of proteins by sedimentation equilibrium in the analytical ultracentrifuge Methods in enzymology, pp. 346–441. Elsevier, Hoboken (1973)
Teng, H., Yamasaki, A., Chun, M.K., Lee, H.: Solubility of liquid co2in water at temperatures from 278 k to 293 k and pressures from 6.44 mpa to 29.49 mpa and densities of the corresponding aqueous solutions. J. Chem. Thermodyn. **29**(11), 1301–1310 (1997)
Tichacek, L., Kmak, W., Drickamer, H.: Thermal diffusion in liquids; the effect of non-ideality and association. J. Phys. Chem. **60**(5), 660–665 (1956)
Wales, M., Williams, J., Thompson, J., Ewart, R.: Sedimentation equilibria of polydisperse non-ideal solutes experiment. J. Phys. Chem. **52**(6), 983–998 (1948)
Whitson, C. H., Belery, P., et al.: Compositional gradients in petroleum reservoirs. In: University of Tulsa centennial petroleum engineering symposium, Society of Petroleum Engineers (1994)
Williams, J., Van Holde, K.E., Baldwin, R.L., Fujita, H.: The theory of sedimentation analysis. Chem. Rev. **58**(4), 715–744 (1958)
Wooding, R.: Steady state free thermal convection of liquid in a saturated permeable medium. J. Fluid Mech. **2**(3), 273–285 (1957)
Xu, K., Bonnecaze, R., Balhoff, M.: Egalitarianism among bubbles in porous media: an ostwald ripening derived anticoarsening phenomenon. Phys. Rev. Lett. **119**(26), 264502 (2017)
Xu, K., Mehmani, Y., Shang, L., Xiong, Q.: Gravity-induced bubble ripening in porous media and its impact on capillary trapping stability. Geophys. Res. Lett. **46**(23), 13804–13813 (2019)
Zhao, H., Brautigam, C.A., Ghirlando, R., Schuck, P.: Overview of current methods in sedimentation velocity and sedimentation equilibrium analytical ultracentrifugation. Current Protocols Protein Sci. **71**(1), 20 (2013)